Fuel 319 (2022) 123718

Contents lists available at ScienceDirect

Fuel

journal homepage: www.elsevier.com/locate/fuel

Effect of helical fins on the combustion performance in a micro-step combustor

Zheng Zhang [a], Wubingyi Shen [c], Wei Yao [a,b,*], Qiu Wang [a], Wei Zhao [a,b]

[a] State Key Laboratory of High Temperature Gas Dynamics, Institute of Mechanics, Chinese Academy of Sciences, Beijing 100190, PR China
[b] School of Engineering Science, University of Chinese Academy of Science, Beijing 100049, PR China
[c] School of Aerospace Engineering, Xiamen University, Xiamen 361102, PR China

ARTICLE INFO

Keywords:
Micro-combustion
Helical fin
Combustion performance
Conjugate heat transfer
Mixing

ABSTRACT

This study proposed a novel helical-fin-assisted micro-step Helix combustor to improve the performance of micro-combustors under high flow rates. The effects of the helical fins on the flow and combustion characteristics were analyzed with the aid of detailed hydrogen-air chemistry and a conjugated heat transfer mode. The performance of the proposed Helix combustor and the conventional micro-step combustor was compared. With the increase of the inlet velocity, two flame stabilization modes can be identified, i.e., the helical-fin-anchored flame and the traditional step-stabilized flame. The intensified heat transfer conjugation between the flame and helical fins enables the ignition and stabilization of the premixed flame before the inlet velocity reaches 34 m/s. The swirl flow induced by the helical fins reduces the length of the recirculation zones behind the step while augmenting the mixing between the hydrogen and the high-temperature products, which finally improves the combustion efficiencies. The helical-fin-anchored flame is preferred for thermo-electric/photovoltaic systems due to the uniform yet high wall temperature, as well as higher thermal efficiency. Meanwhile, the step-stabilized flame in the proposed combustor shows advantages of higher combustion efficiency and higher exhaust temperature for micro- engines under higher inlet velocities.

1. Introduction

Micro-scale combustion has attracted much attention recently as a promising heat and power source for small-scale apparatus. Compared with the commonly utilized micro-scale batteries, micro-scale combustion has advantages in energy density, output power, and recharge time. Micro-scale combustion has applicability in a diversity of fields, such as thermoelectric or thermophotovoltaic systems, engines or turbines, and fuel reformers [1]. However, issues arise when it comes to the miniaturization of the combustion system. The increase of surface-to-volume leads to strong thermal and chemical coupling between the flame and wall, the residence time for reaction and mixing between reactants reduces significantly, and the mixing intensity moderates at a relatively low Reynolds number in micro-scale combustors. These issues lead to weak flame stability. Several unsteady flame behaviors have been observed in previous studies, such as oscillating flames [2,3], flames with repetitive extinction and ignition (FREI) [4,5], rotating/spinning flames [6,7], flame streets [8], and symmetry-breaking flames [9,10]. Consequently, the performance regarding the flame stability and combustion efficiency will be significantly changed in micro-combustors.

The heat transfer conjugation between the flame and the wall as an unavoidable effect on the flame stability in the micro-scale combustion has received plentiful research. Unlike the traditional single direction heat-loss effects considered in thermal quenching of the flame in narrow channels [11], the bidirectional heat transfer between the gas and solid phases has been comprehensively investigated in micro-combustors to reveal mechanisms for flame instability and to explore strategies for flame stabilization. Several unique flame behaviors such as slow-burning flame [12] and repetitive ignition and extinction dynamic flame [4] are found in narrow channels due to the contributions of heat conjugation between flame and wall. The “excess enthalpy” combustion realized through heat recirculation between the high-temperature exhaust and the unburned mixture significantly extends flammability limits and stability of the flame in micro-combustors [13]. Following those studies, the heat management strategies in terms of heat loss and recirculation are further investigated [14]. The wall materials with anisotropic thermal conductivity were applied to enhance the heat

* Corresponding author at: State Key Laboratory of High Temperature Gas Dynamics, Institute of Mechanics, Chinese Academy of Sciences, Beijing 100190, PR China.
E-mail address: weiyao@imech.ac.cn (W. Yao).

https://doi.org/10.1016/j.fuel.2022.123718
Received 12 January 2022; Received in revised form 19 February 2022; Accepted 25 February 2022
Available online 9 March 2022

Nomenclature

A	cross-sectional area of the channel, m^2
C	reaction progress variable
C_p	specific heat, J/(kg•K)
C_w	specific heat of the wall, J/(kg•K)
D_1, D_2, D_3	inner and outer diameters of the combustor, mm
dS_f	vector of surface element
h	enthalpy of the fluid, J/kg
h_o	convective heat transfer coefficient, W/(m^2 • K)
h_g	enthalpy of species$g$, J/kg
h_r	radiant heat flux, W
h_1	height of the fins, mm
H_c	combustion enthalpy of hydrogen, J/kg
J_g	mass diffusion flux of species$g$, kg/(m^2 • s)
L_1, L_2, L_3	length of the different parts of the combustor
Le	Lewis number
L_n	nominal combustor length
$\dot{m}_{H_{2,outlet}}$	mass flow rate of hydrogen integrated over outlet, kg/s
$\dot{m}_{H_{2,Z}}$	mass flow rate of hydrogen integrated over z slices, kg/s
$\dot{M}_{H_2}$	mass flow rate of hydrogen at the inlet, kg/s
p	pressure, Pa
R	gas constant
R_c	hydrogen consumption ratio
R_g	production rate of species$g$, kg/(m^3 • s)
R_{H_2}	consumption ratio of hydrogen, kg/(m^3 • s)
R_p	hydrogen penetration ratio
S	area of the cell surface in axial direction
T_∞	ambient temperature, K
t	time, s
T	flame temperature, K
T_{out}	average exhaust gas temperature at outlet, K
T_{wall}	temperature of the wall, K
$T_{w,o}$	outer surface temperature of the wall, K
u_i, u_j, u_k	velocity component, m/s
$\boldsymbol{V}$	velocity vector
V_a, V_r	axial and radial components of velocity, m/s
V_{in}	inlet velocity, m/s
w_1	width of the fins, mm
x_i, x_j, x_k	coordinates in rectangular coordinate system
y	transverse coordinate
Y_g	mass fraction of species g

Greek symbols

ΔH_{nor}	normalized total enthalpy change
ε	surface radiative emissivity
η_c	combustion efficiency
η_r	conversion ratio of chemical energy to radiant heat
λ	thermal conductivity of the gas mixture, W/(m • K)
λ_w	thermal conductivity of the wall, W/(m • K)
μ	dynamic viscosity, kg/(m • s)
ρ	density, kg/m^3
ρ_w	density of the wall, kg/m3
τ	cell volume
σ	Stephan-Boltzmann constant, W/(m^2 • K^4)
ω	edge length of the bluff-body
ω_{mag_xy}	magnitude of vorticity, s^{-1}

Abbreviation

Helix	micro-step combustor with helical fins
MPTV	micro-thermophotovoltaic
RZ	recirculation zone
Step	original micro-step combustor

recirculation and reduce the heat loss [15]. The concept of a multi-channel combustor [16,17] was utilized to strengthen the preheating by forming a counter-flow between burnt products and unburnt reactants. The micro-combustor filled with porous mediums [18] and micro-pin–fin arrays [19] is proposed for the micro-thermophotovoltaic (MTPV) system, where the energy conversion efficiency improved significantly with the contributes of them in enhancing heat recirculation and expanding reaction zones. The high surface-to-volume ratio also renders noticeable chemical interactions between the flame and wall in the micro-combustor, facilitating surface catalytic combustion that is ignited at a much lower temperature than gas-phase combustion [20,21]. Because of that, the heat recirculation combustor with coupled catalytic and gas-phase combustion are favorable to sustain a stable flame under a high heat-loss ratio [22,23].

However, the benefits of heat recirculation and catalytic combustion in strengthening reactivity and reducing chemical time diminish with an increasing flow rate as the heat and species transported from flame to wall are limited by insufficient residence time. Various flame holders are adopted to stabilize the flame in micro-combustors. The flow separation near the flame holders induces flow recirculation zones, which provide high-temperature radicals and low-velocity bays for flame stabilization. Wan et al. [24] found that the central bluff-body in a planar micro-combustor greatly extends the blow-off limit of the hydrogen/air premixed flame. Bagheri et al. [25] compared performances of micro-combustors with different type bluff-bodies, where the central bluff-body-assisted cases exhibit higher exhaust temperature, lower wall temperature, and poorer flame stability compared to the wall-blade ones. Niu et al. [26] investigated the flame stability of the central bluff-body and found that the blow-off limit increases as the blockage ratio increases from 0.2 to 0.4. A variant of central bluff-body which with slits on both sides is proposed by Yan et al. [27] to extend the reflux behind the bluff-body and enhance the combustion efficiency. The dual-convex fin was utilized by Pan et al. [28] to strengthen hydrogen consumption in micro combustors operated at relatively low velocities. The cavity structure as a frequently-utilized flame holder in supersonic combustors [29] was also introduced in the design of micro-combustors. Li et al. [30] found that the mutual assistant coupling of heterogeneous and homogeneous combustion can boost the consumption rate of methane and broaden the operation range of the stable flame in a micro-combustor with cavity and catalyst segments. Wan et al. [31] investigated the combustion characteristics of the hydrogen/air premixed flame in a dual wall-cavity assisted micro-combustor, where no blow-off was observed under the examined inlet velocities. The flame was split near the tip under high inlet velocities, drastically reducing combustion efficiency. Besides, central bluff-bodies [32] and guide vanes [33] were combined with the cavity to suppress the split of the flame and improve the combustion efficiency of the cavity-based micro-combustor through strengthening the flow recirculation and mixing.

The backward step as a favorable flame holder has also been adopted and extensively investigated since the primary stage of the micro-combustion technology development. Yang et al. [34] compared the H_2/air premixed flame behavior and wall temperature of the micro-cylindrical combustors with and without a step, and concluded that the step anchored the flame in a wide operational range with a high yet uniform wall temperature, which is preferred for the applications based on thermal energy from the outer wall such as thermophotovoltaic, thermoelectric, and fuel reformer. The stability of CH_4/air premixed flame was investigated in the stepped micro-combustors by Kumar et al. [35,36]. Unlike the H_2/air premixed flame anchored by the recirculation zone behind the step [34], the CH_4/air premixed flame is more likely to

stabilize downstream of the recirculation zone and exhibits oscillations or even blow-out under relatively high inlet velocities. Zarvandi et al. [37] found that the added H_2 provided vital radicals to ignite and stabilize the CH_4/air premixed flame near the step wall and led to a more uniform wall temperature. Besides, the multi-stages step was proposed by Khandelwal et al.[36] and Peng et al. [38] to improve the flame stability of CH_4/air flame and stabilize the flame position of the H_2/air flame, respectively. Yilmaz et al. [39] investigated the performance of micro-combustors with backward step and cavity, respectively. The results show that the backward-step combustor has superiority in wall temperature distribution and radiant energy conversion. The studies of E et al. [40] and Yang et al. [34] on stepped micro-combustors show that the exit temperature and combustion efficiency decrease with the increase of inlet velocities, whereas the wall temperature eventually rises to a quasi-stable stage, suggesting a limit of the output thermal power [41].

Therefore, the research interest for stepped micro-combustors mainly focused on wall temperature distribution and energy output under moderate flow rates, with the purpose of applications in MTPV or micro-thermoelectric systems. The combustion performance under higher flow rates by using backward steps and their potential in micro-engines have rarely been explored. It was pointed out that improving the exhaust gas temperature rather than the wall temperature is the key to achieving higher efficiency of the micro-engine system under high flow rates [42,43]. As the merits of the backward step in stabilizing flame have been proved in the previous study [34,44], improving the combustion efficiency should be crucial for enhancing exhaust gas temperature. In this study, a newly designed micro-step combustor with helical fins in the inlet channel is investigated. The helical fins are expected to enhance preheating effect of the inlet channel [45,46] and strengthen the mixing between the fresh mixture and the burned gas near the step wall through the activated swirl flow [35,47]. Even though the swirl flow has been reported to broaden the stability limits in micro-step combustors [30,41], its effect in improving combustion efficiency, especially under high flow rates, has not been comprehensively investigated. Therefore, the combustion characteristics and the performances of the helical fin enhanced micro-step combustor are numerically investigated and compared with a conventional micro-step combustor under increasing inlet velocities. The characteristics of the flame-wall coupling, flame-flow interactions, and the mixing of reactants are analyzed to reveal the underlying mechanisms of the improvements.

2. Numerical methodology

2.1. Combustor geometry

The micro-step combustor with helical fins mounted on the inner wall of the inlet channel is shown in Fig. 1. The inner diameter of the inlet channel before the step wall is $D_1 = 2mm$ and the inner diameter of the chamber behind the step are$D_2 = 4mm$, both of them are enveloped by the solid wall with an outer diameter of$D_3 = 6mm$. The length of the inlet channel and total length of the combustor are $L_1 = 7mm$ and$L_2 = 27mm$, respectively. The helical fins are created by spirally revolving a rectangle along four helical trajectories equally embedded in the inner wall of the inlet channel. The pitch distance of the helical trajectory is$L_3 = 6.28mm$. The width and height of the rectangle are $w_1 = 0.3mm$ and$h_1 = 0.3mm$, respectively. The micro-step combustor with the same dimensions but without helical fins referring to the experiments of Li et al. [48] is investigated for comparison. For convenience, the micro-step combustor with helical fins is called Helix combustor, and the Li's micro-step combustor is called Step combustor.

2.2. Numerical configurations

The H_2/air premixed flame and the conjugated heat transfer within the Helix combustor are modeled in the three-dimensional (3-D) domain shown in Fig. 1. The reacting flow in the combustor is modeled by solving transient Navier-Stokes equations together with transport equations of enthalpy, species, and turbulence quantities. The following assumptions are made, (a) radiant heat transfer within solid and gas regions are ignored [49], (b) work done by viscosity and pressure are omitted, (c) gravity effect is ignored, (d) Dufour effects are ignored. The final governing equations are given as follows.

$$\frac{\partial \rho}{\partial t} + \frac{\partial \rho u_i}{\partial x_i} = 0 \tag{1}$$

$$\frac{\partial \rho u_j}{\partial t} + \frac{\partial}{\partial x_i}\left(\rho u_i u_j\right) = \frac{\partial}{\partial x_i}\left[\mu\left(\frac{\partial u_j}{\partial x_i} + \frac{\partial u_i}{\partial x_j}\right)\right] - \frac{2}{3}\frac{\partial}{\partial x_i}\left(\mu\frac{\partial u_k}{\partial x_k}\right) - \frac{\partial p}{\partial x_j} \tag{2}$$

$$\frac{\partial \rho h}{\partial t} + \frac{\partial}{\partial x_i}\left(\rho u_i h\right) = \frac{\partial}{\partial x_i}\left(\frac{\lambda}{C_p}\frac{\partial h}{\partial x_i}\right) + \sum_g\left[\frac{\partial}{\partial x_i}\left(h_g J_g\right)\right] + \sum_g h_g R_g \tag{3}$$

$$\frac{\partial \rho Y_g}{\partial t} + \frac{\partial}{\partial x_i}\left(\rho u_i Y_g\right) = \frac{\partial J_g}{\partial x_i} + R_g \tag{4}$$

where ρ is the density, u the velocity and p the pressure, the subscript$i$, j and k presenting three directions of Cartesian coordinates; μ and λ are the effective dynamic viscosity and thermal conductivity of the mixture; h and h_g denote the total enthalpy of the mixture and gas species$g$; C_p is the specific heat of the mixture;Y_g, J_g and R_g are the mass fraction, the mass diffusion flux, and the net production rate of gas species, respectively. The ideal gas law is employed to close the Eqs. ((1)–(4)),

$$p = \rho RT \tag{5}$$

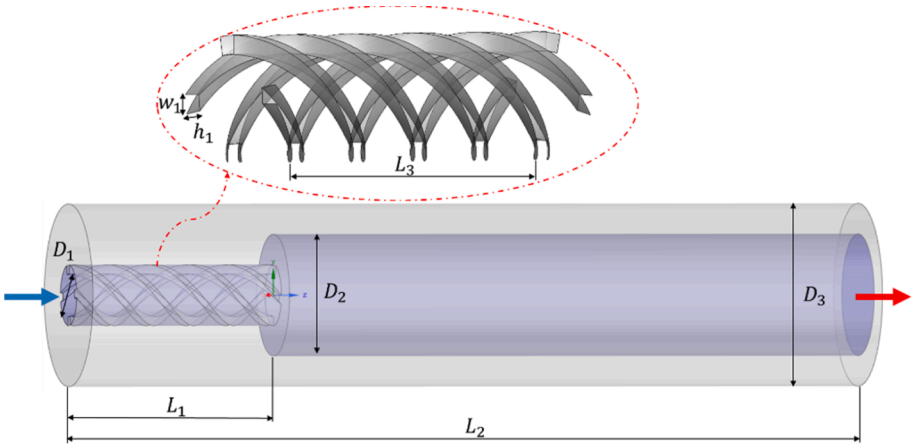

Fig. 1. Schematics of the combustor with helical fins.

where R is the gas constant and T is the temperature of mixtures. Given the high inlet velocities investigated in this study (the minimum Reynolds number is larger than 2400) and the swirling flow induced by helical fins, the turbulent effect is modeled by the realizable $k-\epsilon$ turbulent model, whose applicability has been proved in previous numerical studies on micro-combustors with swirling flows [46,50,51]. The turbulent combustion is modeled with the finite rate model, where the finite chemical rate is calculated based on a hydrogen oxidation mechanism containing 19 reversible reactions and nine species [52]. The thermophysical and transport properties of individual species, including thermal conductivity, mass diffusivity, and viscosity, are calculated based on CHEMKIN-format thermodynamic [53] and transport database [54]. Mixture properties are calculated with the idea-gas mixing law.

The heat transfer coupling between the solid wall and the flame is modeled via solving the solid heat transfer equation as well,.

$$\frac{\partial(\rho_w C_w T_{wall})}{\partial t} = \frac{\partial}{\partial x_i}\left(\lambda_w \frac{\partial T_{wall}}{\partial x_i}\right) \tag{6}$$

where ρ_w, C_w are the density, specific heat of the wall, λ_w is the conductivity of the wall, and T_{wall} denotes the wall temperature. The wall material is assumed to be stainless steel, with the constantρ_w, C_w, and λ_w of 8000kg/m^3, 0.46kJ/(kg•K), and 13.5 W/(m•K) [55].

The H_2/air mixture with uniform velocity is fed through the inlet boundary. The equivalence ratio and initial temperature of the mixtures are fixed at 0.5 and 300 K, respectively. Zero-gradient condition with ambient pressure is applied on the outlet of the combustor. On the interfaces between the fluid and solid regions, the coupled thermal boundary is imposed with restrictions of equal heat flux and temperature in the neighbor sides of the two regions. The non-slip and zero-gradient conditions are specified on the interfaces for velocity and species boundaries. The heat flux from the outer wall to the ambient is determined by.

$$q = h_o\left(T_{W,O} - T_\infty\right) + \varepsilon\sigma\left(T_{W,O}^4 - T_\infty^4\right) \tag{7}$$

where h_o is the natural convective heat transfer coefficient, $T_{W,O}$ is the local temperature of the outer wall, and T_∞ are the ambient temperature, ε is the wall emissivity, and σ is the Stefan– Boltzmann constant. A simplified equation, $h_o = 1.42\left(\frac{T_{W,O}-T_\infty}{L}\right)^{1/4}$ [56] is employed for free convection on the vertical cylindrical outer surface. The $T_\infty = 300$K and $\varepsilon = 0.5$ are adopted [48].

The turbulence, combustion, and conjugate fluid–solid heat transfer are solved by the commercial software ANSYS-Fluent v14. A pressure-based SIMPLE algorithm is used to resolve the velocity–pressure coupling. The second-order upwind scheme is applied for the spatial discretization, and the time marching is realized by the first-order implicit scheme. The solution is converged at scale residuals smaller than 10^{-6} for energy and 10^{-3} for the others. The flame is ignited by patching a high-temperature zone in the recirculation zone behind the step wall.

2.3. Grid independence and model validation

Hex-dominant mesh is adopted with partial refinement in regions near the helical fins and step wall. Three sets of grid systems are generated to ensure grid convergence. As shown in Fig. 2(a), the mass fraction of H_2 and temperature distributions along the z-axis of the Helix combustor at an inlet velocity of 34 m/s are compared between fine, medium, and coarse meshes with 6.37, 2.63, and 0.94 million cells, respectively. The discrepancies between different meshes are inconspicuous, especially for the medium and fine meshes, indicating that grid convergence has been achieved. The results by the medium mesh with an average size of 60 μm are used in the subsequent analysis to satisfy the accuracy and save the computational cost. Moreover, the experimental data of the outer wall temperature of the Step combustor is collected from the experiments of Li et al. [48] to validate numerical results of the Step combustor utilized in the experiments. Given the low inlet velocity of 4 m/s applied in the experiment, the Reynolds number (Re) based on the combustion chamber diameter $D_2 = 4mm$ is around 880 which indicating the laminar regime for the flow. However, the study of Kuo and Ronney [57] on a micro-scale "Swiss-roll" combustor suggests that the turbulent transport modeling is required for Re larger than 500 to predict heat recirculation accurately. To confirm that, the numerical results obtained using laminar and turbulent models are compared with the experimental results in Fig. 2(b). The turbulent model obtains a smaller difference between the numerical and experimental results than the laminar model, especially for the high-temperature region. Because the Reynolds number is much higher than 500 for the high inlet velocity investigated in this study, the realizable $k-\epsilon$ turbulent model is preferred. It can be seen that the tendency of the measured outer wall temperature has been well captured by the turbulent simulation results. The maximum discrepancy of 3.15% between them is found near the inlet side, which can be interpreted by the deviation of the thermal boundary modeled with Eq. (7) with the actual heat conduction through the long metal pipe in the experiment [48]. The metal heat conduction usually has a higher heat sink effect and thus may produce a lower temperature near the inlet. Overall, the predicted outer wall temperature with the turbulent model shows reasonable agreements with the experimental data.

3. Results and discussion

3.1. Flame patterns under various inlet velocity

Fig. 3 shows the contours of temperature and mass fraction of OH (Y_{OH}) at various inlet velocities V_{in} for the Step and Helix combustors.

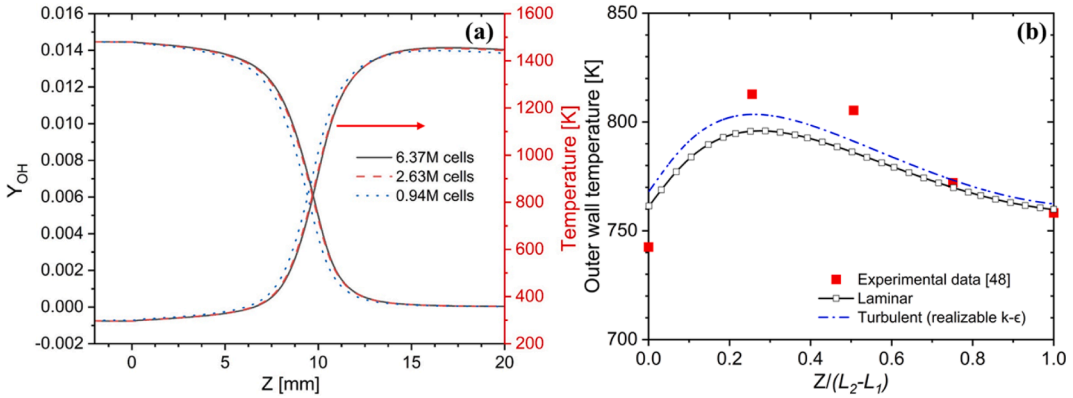

Fig. 2. (a) Grid independence study, and (b) comparison of the outer wall temperature between numerical and experimental results at an inlet velocity of 4 m/s.

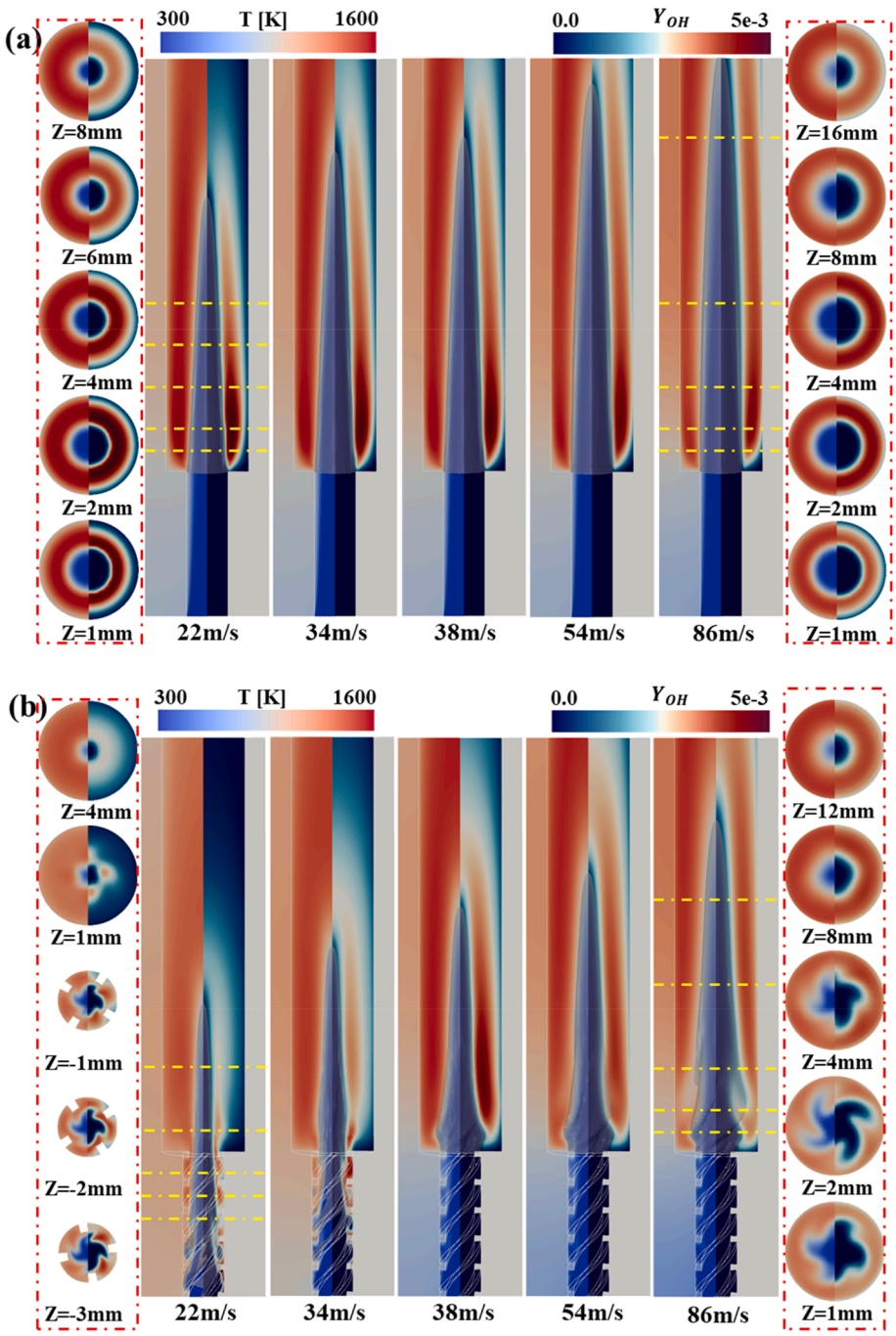

Fig. 3. (left) Temperature and (right) OH contours on the central plane of Y = 0 and various Z slices (the positions are indicated by yellow dash-dot lines) with overlaid flame surfaces (transparent surfaces) of (a) Step and (b) Helix combustors at increasing inlet velocities. (For interpretation of the references to color in this figure legend, the reader is referred to the web version of this article.)

The contours of reaction progress variable $C = 0.5$ [58] are depicted to show the flame fronts for both micro-combustors. The progress variable is defined based on the main products,.

$$C = \frac{(Y_{H2O} + Y_{OH}) - (Y_{H2O} + Y_{OH})_{min}}{(Y_{H2O} + Y_{OH})_{max} - (Y_{H2O} + Y_{OH})_{min}} \tag{8}$$

A similar flame behavior can be found for both combustors, i. e., the flame zone indicated by OH retreats to the thinner zones near the wall with the increase of V_{in}. Such tendency was also observed in previous studies of the step-based micro-combustors [59,60], and can be interpreted by the decreasing of residence time under high V_{in}. There are significant differences between the Step and Helix combustors despite the above-mentioned behavior. At relative low V_{in}, the flame root is anchored by helixes and the reaction zone extends into the inlet channel, while the traditional step-stabilized flame is anchored by the recirculation zone behind the step. Compared with the Step combustor, the flame front becomes shorter, and the wall temperature of the inlet channel increases significantly. As V_{in} increases, the flame anchored by the helical fins is blown off and transits to the step anchored mode as in the Step combustor. The flame surface is deformed from a smooth cone into a shorter spiral cone. The temperature and OH distributions on the Z-slices form a special "quatrefoil" shape and a regular "annulus" shape in the Helix and Step combustors, respectively. As V_{in} increases to 86 m/s, the flame tip starts to extend out of the Step combustors and the flame

tip split at the outlet before the occurrence of "tip-opening" [31]. No tip-opening occurs for the Helix combustor, even at a high velocity ofV_{in} = 86m/s..

3.2. The helical fin anchored mode

Variations of the axial velocity (V_a) and the net consumption rate of hydrogen (R_{H_2}) of the helical fin anchored flames with increasing inlet velocities are shown in Fig. 4. A large amount of hydrogen is consumed within the inlet channel of the Helix combustor and the largest R_{H_2} is obtained near the helical fins rather than the shear layer behind the step in the Step combustor. With the increase of V_{in}, the flame anchoring position recedes, and meanwhile, the reaction intensity behind the step increases. The gas expansion due to heat release and the blockage effect of the helical fins drive V_a to be much higher in the Helix combustors than in the step combustors. With higher axial velocities and stronger shear flow in the Helix combustor, larger recirculation zones (RZ, denoted by the solid yellow lines of $V_a = 0$) are formed behind the step. With the increase of V_{in}, the axial velocity increases and the length of RZ shrinks gradually in the Helix combustor, while RZ extends in the Step combustors. The shrinkage of RZs in the Helix combustor with increasing V_a will be interpreted in the following section. Besides, it should be noted that the Helix combustor does not fully taken the advantage of large RZs since the flame are anchored by the fins and most of the hydrogen are burnt before the step.

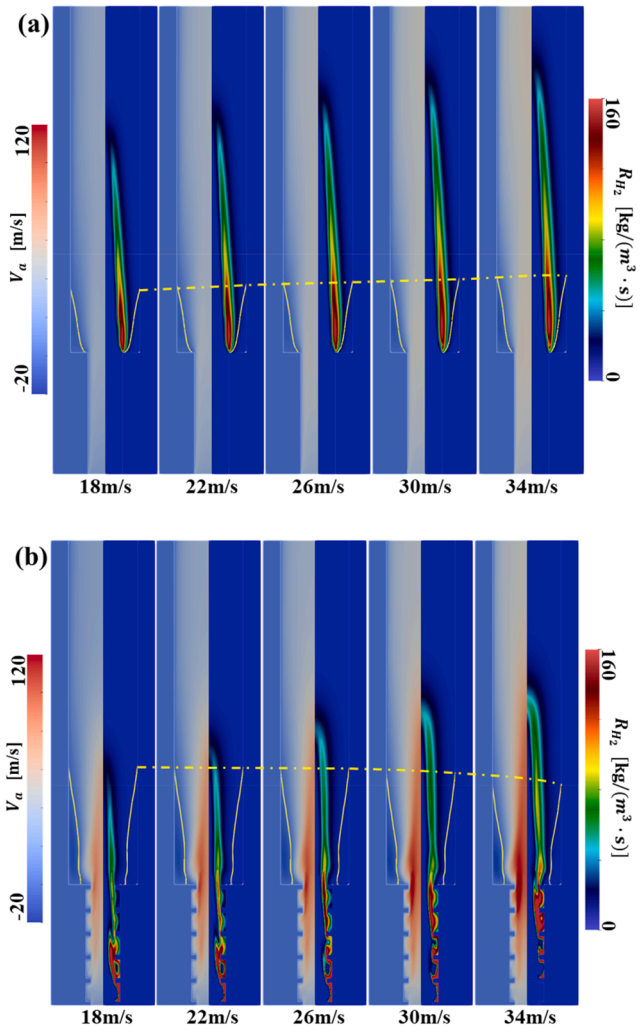

Fig. 4. Variations of the (left) axial velocity (V_a) and (right) net consumption rate of hydrogen (R_{H_2}) for the helical fin anchored flames in Helix combustors and their counterparts in Step combustors with increases of inlet velocities. The contour lines of $V_a = 0$ (solid yellow lines) are overlaid to indicate the flow recirculation zones, and the trend of their heights is depicted by the yellow dash lines. (For interpretation of the references to color in this figure legend, the reader is referred to the web version of this article.)

To illustrate the flame anchoring mechanism of the helical fins, the temperature contours of the solid wall and the distributions of HO_2 under V_{in} = 34 m/s are shown in Fig. 5. The radical HO_2 is the main product before ignition and also the major reactant for chain-branching reactions [61], which starts from the linear chain reaction H + O_2(+M) = HO_2(+M) at relatively low temperature [62]. The ignition of the helical fin anchored flame can be divided into two major stages, the induction stage (from Z = −7 to Z = −4 mm) and the self-sustaining stage. At the induction stage, the HO_2 is firstly formed near the hot inner surface of the helical fins where the mixture has been heated to activate low temperature reactions. Further downstream, the wall temperature increases, and the accumulated HO_2 near the fins during the induction stage is consumed to generate H and H_2O and release heat for chain reactions. The released heat sustains the flame in the self-sustaining stage, where a large amount of HO_2 is formulated in the low-temperature central zone as shown on the Z = −1 mm slice. The observation that wall surfaces ignited the premixed hydrogen flame with a temperature higher than 1000 K coincides with the previous study [63]. Thus, the temperature of the helical fins is essential for flame stabilization in the inlet channel. From Fig. 5, it can be found that the helical fins gain higher temperature than the inlet channel walls when heat is transformed from flame to solid wall, and that trend inverts in the upstream preheating region. It implies that the helical fins can build up a stronger heat conjugation between the wall and the flame, which promotes the heat feedback from the post-flame zone to the fresh mixture to ignite the flame near the fins and render a higher flame stabilization limit in the inlet channel consequently.

The inner wall temperature (T_{inner}) of the inlet channel for the helix combustor is shown in Fig. 6. As V_{in} is increased from 22 m/s to 34 m/s, T_{inner} reduces with the receding of the reaction zone, especially at V_{in} = 34 m/s. The maximum T_{inner} is higher than 1000 K [63]. However, as the V_{in} further increases, the heat feedback through the fins reduces and fails to ignite and stabilize the flame. Once the flame recedes to be anchored by the step wall at velocities higher than V_{in} = 36 m/s, the low T_{inner} no longer permits surface ignition any more.

3.3. The step stabilized mode

As shown in Fig. 7, for step anchored flame in both types of combustors, the flame root is firmly stabilized by the recirculation zone (RZ)

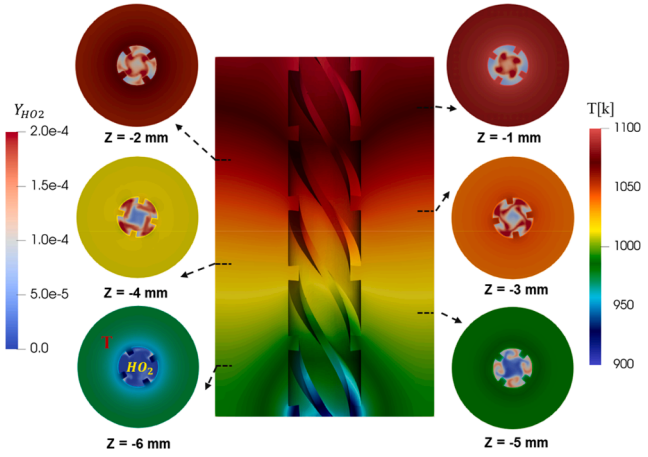

Fig. 5. The ignition process of the helical fin anchored flame at V_{in} = 34 m/s. The wall and flow regions are mapped with temperature and HO_2 respectively in the z-slices and the inlet channel.

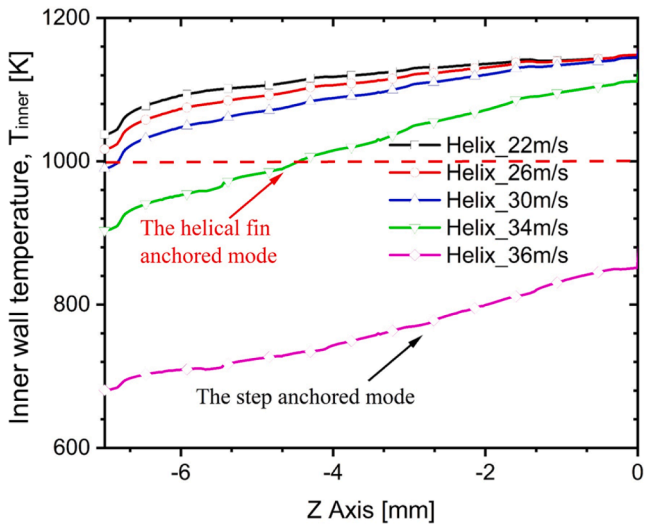

Fig. 6. Inner wall temperature of the inlet channel for the Helix combustor under increasing inlet velocity.

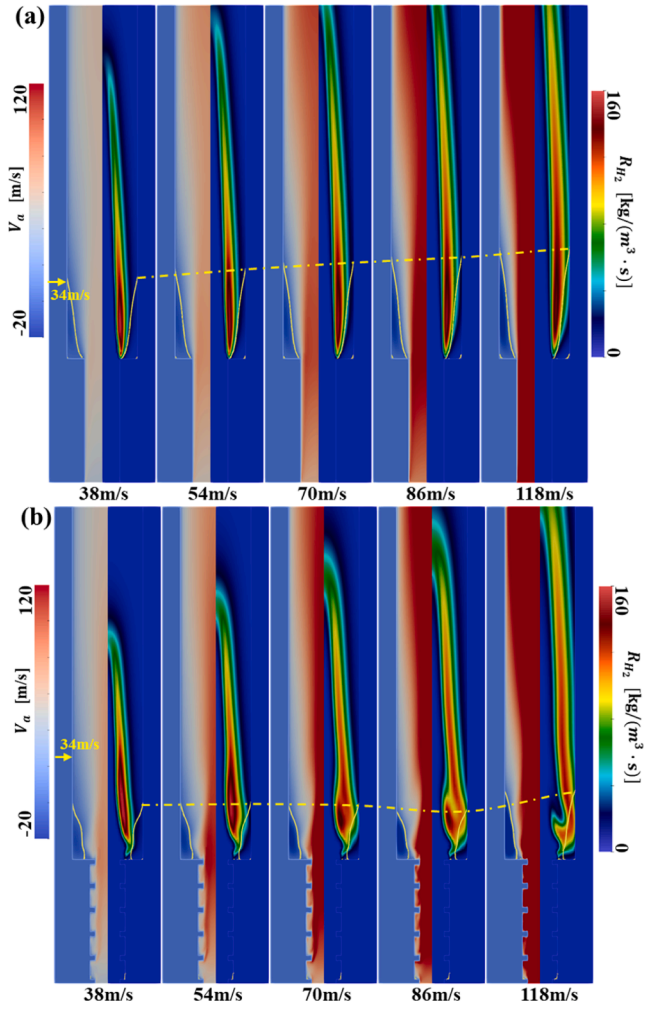

Fig. 7. Contours of the (left) axial velocity (V_a) and (right) net consumption rate of hydrogen (R_{H_2}) for step anchored flames in (a) the Step combustor and (b) the Helix combustor under increasing inlet velocity. The solid yellow line indicates the position of$V_a = 0$. (For interpretation of the references to color in this figure legend, the reader is referred to the web version of this article.)

behind the step. The recirculation zone provides a low-velocity bay with a high temperature and abundant radicals. The flame structures indicated by V_a and R_{H_2} have significant differences between the Helix and the Step combustor, especially for the recirculation zone. Even though higher V_a is observed in the central zone of the Helix combustor, a wider low-velocity region is observed near the recirculation zone. From the distribution of R_{H_2}, thicker reaction zones with rich hydrogen and low velocity is observed in the Helix combustor. The reaction zones penetrate deeper into the recirculation zone in the Helix combustor than in the Step combustor. The length of the recirculation zone in the Helix combustor significantly reduces as the flame transforms from the helical-fin-anchored mode at $V_{in} = 34$m/s to the step-anchored mode at $V_{in} = 38$m/s.

Variations of the magnitude of vorticity $\omega_{mag\_xy} = \sqrt{\omega_x{}^2 + \omega_y{}^2}$ and the reaction rate of hydrogen (R_{H_2}) along the streamlines around the recirculation zone are shown in Fig. 8. For the Step combustor, nearly axisymmetric flow structures were observed and the vorticity is strong on the shear/mixing layer of the recirculation zone. A complex three-dimensional axisymmetric flow structure was produced by the helical fins in the Helix combustor. Because the gas dilatation due to heat release decreases the vorticity, ω_{mag_xy} decreases significantly through reaction regions, especially for the step stabilized flame in the Helix combustor such as the "Helix-38 m/s" and "Helix-86 m/s" cases, where the flame and flow interaction in recirculation zones intensified. The decrease of vorticity near recirculation zones caused by the heat release should be blamed for the significant decrease of the length of RZs for the Helix combustor. Similar observations were also reported in a previous experiment on a larger scale step combustor, where the flame stabilized behind the step reduces the length of the recirculation zone, which can be by up to 50% compared with that in a cold flow [64], since the thermal expansion reduces the shear stress in the axial direction [65]. Similarly, arising of a weak reaction region behind the step of the helical-fin-anchored-flame cases contributes to the decrease of recirculation zones shown in Fig. 4.

The strengthened flow and flame interactions not only effect the shape of recirculation zones in the Helix combustor but also the reactions of hydrogen as demonstrated in Fig. 7 and Fig. 8. The contours ofR_{H_2}, as well as the profiles of major species, reaction rates, and temperature are shown in Fig. 9 to illustrate the effects of helical fins on the flame. The dominant hydrogen-consuming reactions are the chain reactions $O + H_2 = H + OH$ (R2) and $H_2 + OH = H_2O + H$ (R3) [61]. Thus, the profiles of O, OH and H_2 are plotted as the major species. The regular "annulus" type flame surfaces in the step combustor are stretched by the swirl flow to form a "quatrefoil" shape flame in the Helix combustor. The annulus flame has a thinner zone with a higher R_{H_2} near the flame front (denoted by the red line), especially when it approaches the step wall (z = 0). The"quatrefoil" shape flame exhibits a lower R_{H_2} but wider reaction region in the post-flame zone near the wall. From the profiles of reaction rates, most of the hydrogen is consumed through R3, whose reaction rate is determined by the Y_{OH}, Y_{H_2} and temperature. Near the flame front, R_{H_2} increases with temperature and Y_{OH}. As the reaction zone further approaching the wall, R_{H_2} is controlled by Y_{H_2} rather than temperature and Y_{OH} because hydrogen is deficient there. The swirl flow enhances the mixing between the cold fresh mixtures and the high-temperature products, which not only decreases the temperature near the flame front but also increases Y_{H_2} in the postflame zone. Due to such contradictory effects, a wider reaction zone with weaker reactivity is observed in the Helix combustor, especially near the step wall.

To examine the integrated effects of the helical fins on hydrogen transport and reaction, the hydrogen penetration ratio R_p and consumption ratio R_c are compared in Fig. 10 between two types of combustors. R_p is defined as the ratio of the hydrogen mass flux integrated over the surface of the flame front (S_f) from step wall (z = 0) to z = Z and the mass flow rate of hydrogen at the inlet ($\dot{M}_{H_2}$) calculated by$R_p =$

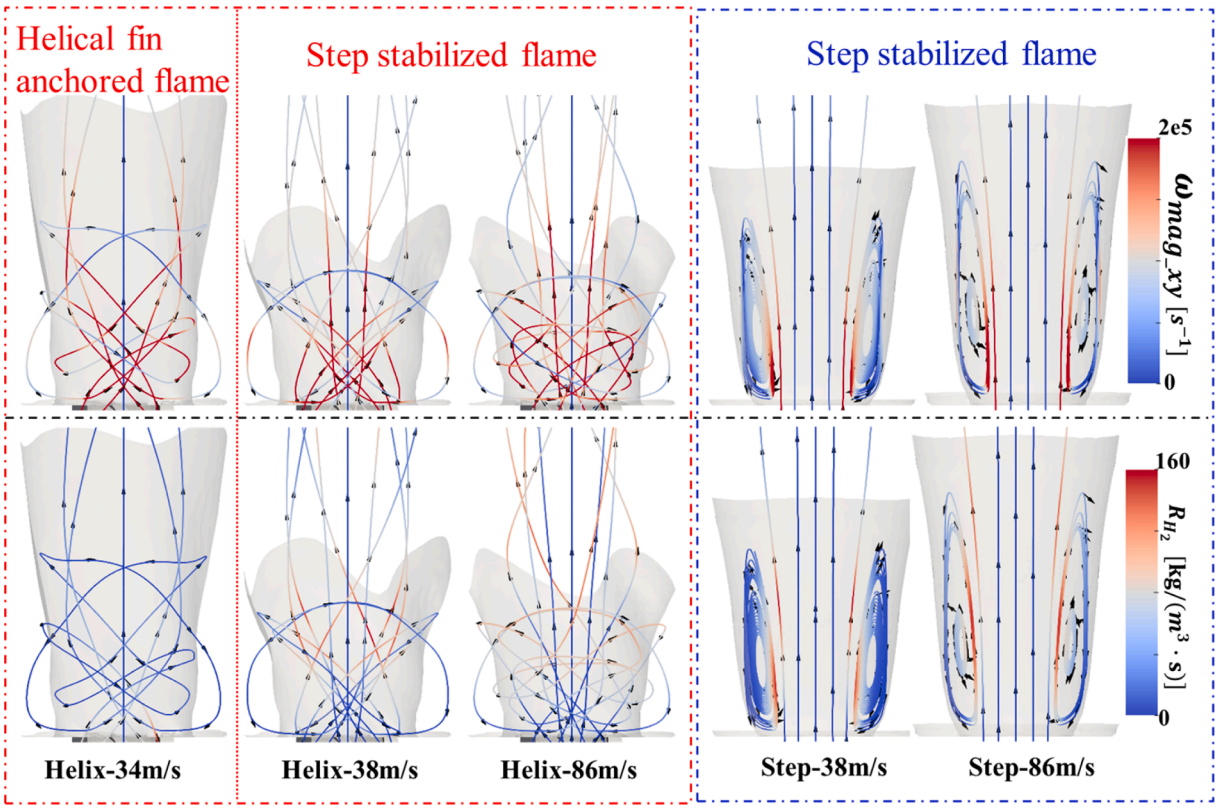

Fig. 8. Streamlines colored by the magnitude of vorticity (up) and the reaction rate of hydrogen (down) near the recirculation zones (illustrated by the isosurfaces of $v_z = 0$ in grey color) the Helix and Step combustors.

$\frac{\int_0^Z \rho Y_{H2} V \cdot dS_f}{\dot{M}_{H_2}}$. R_c is determined by$R_c = \frac{\dot{M}_{H_2} - [\int \rho Y_{H2} V \cdot dS]_z}{\dot{M}_{H_2}}$, where the numerator represents the consumed hydrogen before z = Z. The flame surface of both combustors colored by the hydrogen mass flux through the surface are inserted in Fig. 10 as well. R_p and R_c are compared only for affected region of the helical fins from Z = 1 to 6 mm. Compared with the linear increasing of R_p in the Step combustor, R_p increases rapidly in the Helix combustor, especially near the step wall due to the enhanced mixing by the fins. With the increase of R_p, R_c shows a similar tendency, suggesting a mixing-controlled combustion. The difference between R_p and R_c indicates the amount of hydrogen reacted in the preheat region. $R_c - R_p$ is larger in the Helix combustor than that in the Step combustor due to the enlarged flame surface area by the wrinkling effect, as shown in Fig. 9. Although the recirculation zone is smaller, with a lower temperature and weaker reaction intensity in the Helix combustor, the total amount of hydrogen consumed near the recirculation zone is much higher than the Step combustor due to the enhanced mixing and enlarged wrinkled flame surface area.

3.4. The performances of combustors

The wall temperature and thermal radiation are key aspects for micro-thermophotovoltaic (MTPV) and micro-thermoelectricity systems. The temperature distribution on the outer wall (T_{wall}) is plotted along the z-axis direction as shown in Fig. 11a., T_{wall} has a nearly uniform value of 1080 K for the helical-fin-anchored flame termed as "Helix-22m/s". A similar variation tendency of T_{wall} is observed for both combustors with the step-wall-stabilized flame, where the T_{wall} exhibits an S-shape variation, i.e., rapidly rising near the step wall from a low inlet temperature and finally approaching a flat stage. The variation of total enthalpy (ΔH) through the Z-slices is calculated to indicate wall heat transfer between the flame and the wall. As shown in Fig. 11b, a positive ΔH indicates the preheating effect by the wall, while a negative ΔH implies heat loss. For "Helix-22 m/s", the flame was ignited spontaneously near the inlet and heated the wall subsequently, resulting in a high T_{wall}. At a lower hydrogen flow rate, the smaller decreasing rate of ΔH indicates a weak heat loss and a lower T_{wall} behind the step wall. As V_{in} increases from 22 m/s to 86 m/s, the steeply rising curve of ΔH indicates a strong preheating effect under the step-wall-stabilized mode, which results in the decreasing of T_{wall} before the step. At the same time, improved preheating with the aid of helical fins leads to a lower T_{wall} of the inlet channel, as shown in Fig. 11a.

Fig. 12a compares the variation of radiant heat flux, h_r integrated over the outer wall between the Helix and Step combustors under different inlet velocities,.

$$h_r = \pi d_w \varepsilon \sigma \int T_{wall}{}^4 \theta d_\theta dz \tag{9}$$

The radiant heat flux increases monotonically with the increase of V_{in} and T_{wall} in the Step combustor. For the Helix combustor, h_r increases with V_{in} in most ranges, while a rapid drop appears as V_{in} increases from 34 m/s to 38 m/s, which is caused by the transition of the flame mode. At inlet velocities $V_{in} \leq 34$ m/s with flame anchored by the helical fins, the Helix combustor presents a higher yet uniform T_{wall} compared to the Step combustor. One example is shown in Fig. 11a for the "Helix_22m/s" case. However, under higher inlet velocities, the flame stabilization mode transits from helical-fin-anchored to step-wall-stabilized, where both h_r and T_{wall} of the Helix combustor become lower than the Step combustor. Fig. 12b compares the energy conversion efficiency (η_r) from chemical energy to radiant energy calculated as,.

$$\eta_r = \frac{h_r}{\dot{M}_{H_2} \cdot H_c} \tag{10}$$

where $\dot{M}_{H_2}$ and H_c are the mass flow rate and combustion enthalpy of hydrogen. With V_{in} increases from 18 m/s to 118 m/s, η_r decreases from

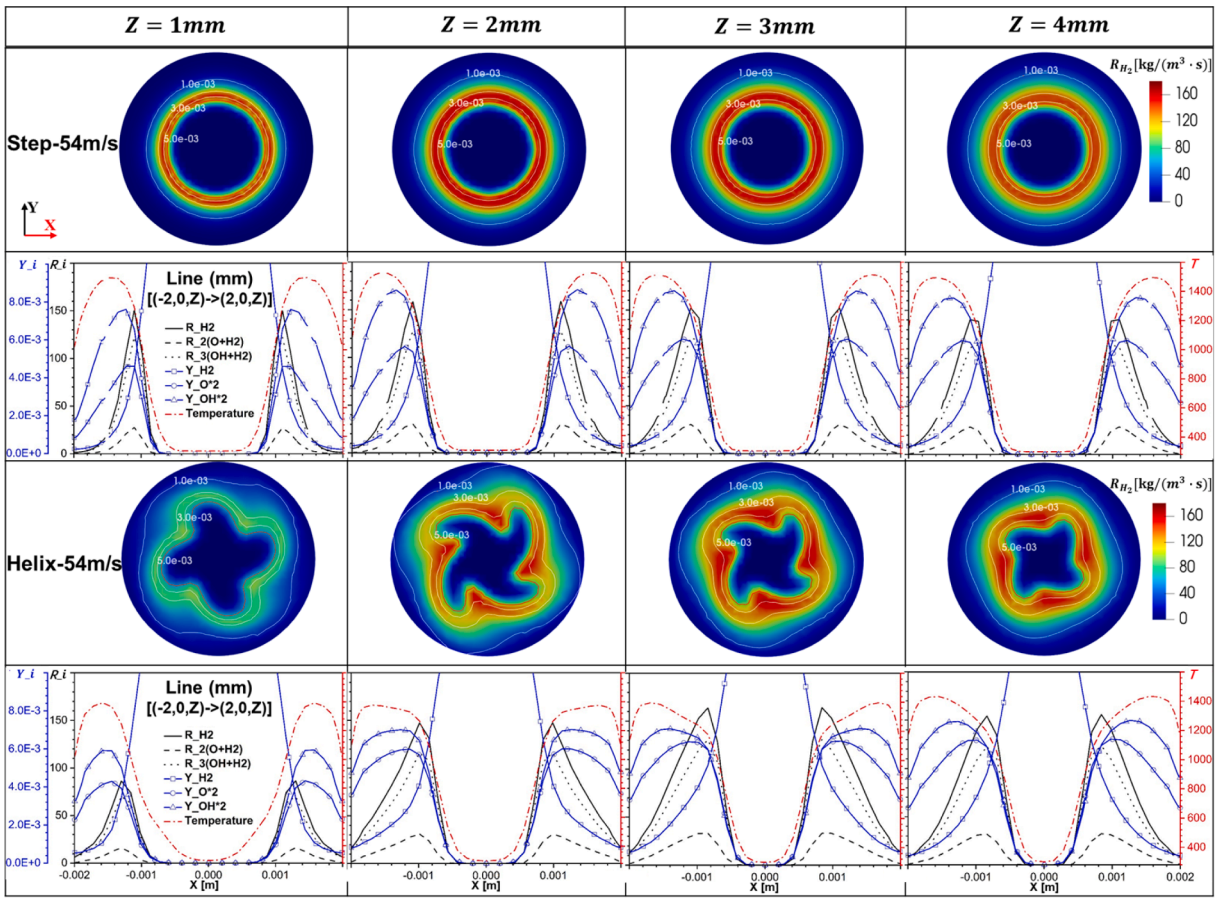

Fig. 9. Contours of hydrogen consumption rate overlaid with contour lines (white lines) of hydrogen mass fraction on various z-slices and the corresponding plots of reaction rates and species over the axis of symmetry in the x-direction. The red line on the slices denotes the flame front. (For interpretation of the references to color in this figure legend, the reader is referred to the web version of this article.)

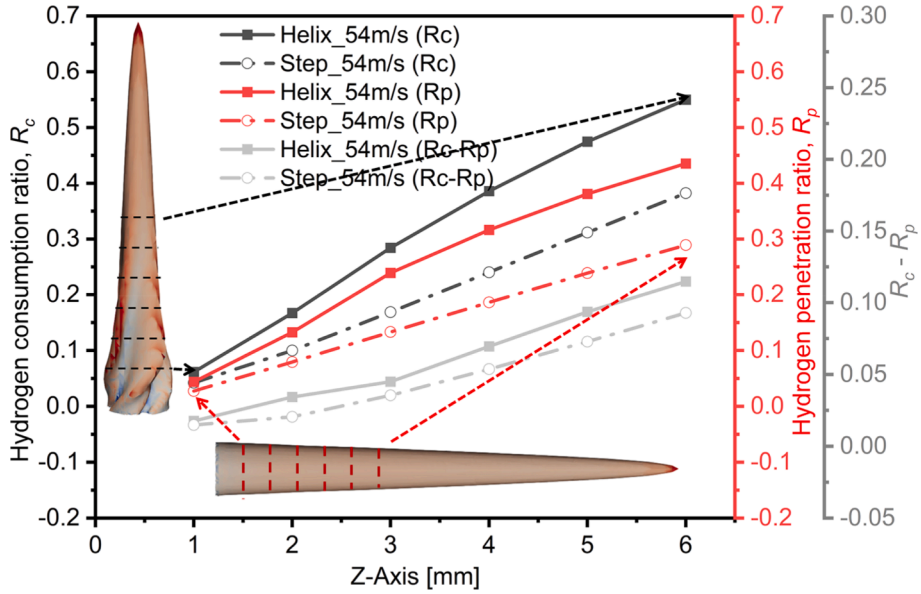

Fig. 10. Comparisons between the Helix and Step combustors for hydrogen consumption (R_c) and penetration (R_p) ratios behind the step wall where flame surfaces colored by the hydrogen mass flux with sampling positions marked by dash lines are inserted.

19.7% to 2.9% in the Helix combustor and from 13.0% to 3.4% in the Step combustor. It implies that the contribution of per unit mass hydrogen on h_r decreases with the increasing mass flow rate. Due to the differences in cross-section area and gas density, mass flow rates are different for the Helix and Step combustors at the same inlet velocity. To evaluate the effect of this difference, variation of h_r and η_r with the mass

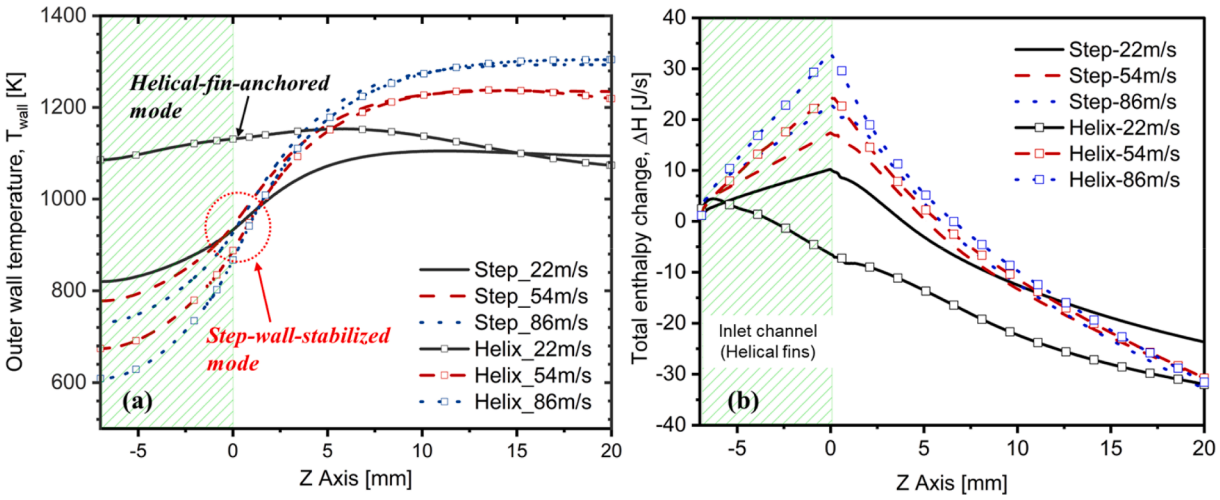

Fig. 11. The variation of (a) average outer wall temperature and (b) total enthalpy change along the z-axis direction for the Step and Helix combustors at various inlet velocities. The green slash lines indicate the inlet channel region before the step wall. (For interpretation of the references to color in this figure legend, the reader is referred to the web version of this article.)

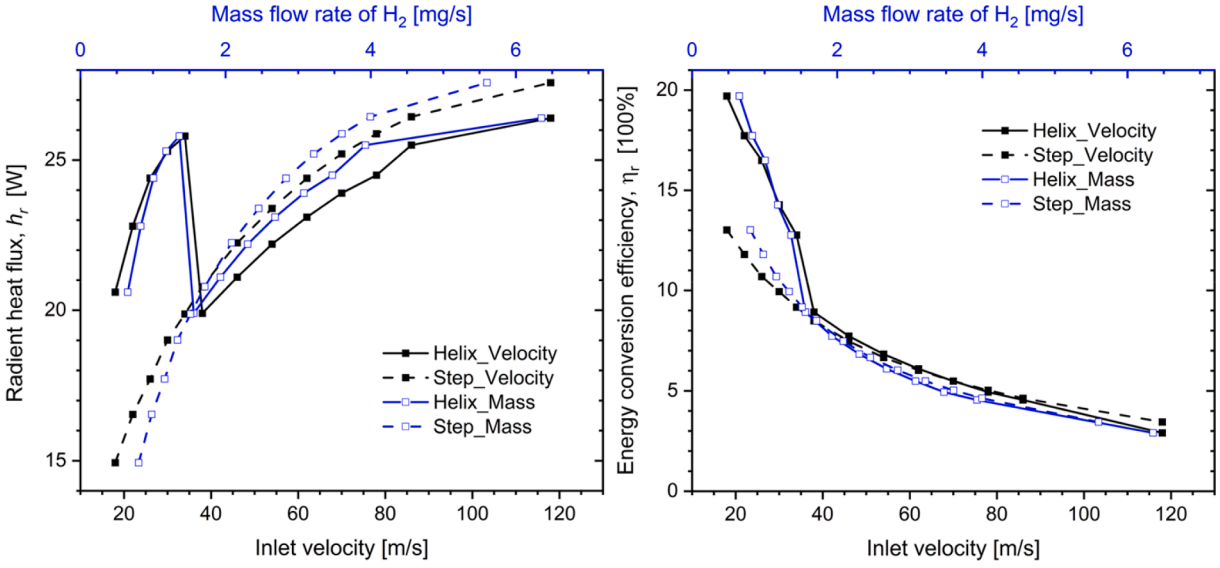

Fig. 12. The radiant heat flux and energy conversion efficiency of the Helix and Step combustors at increasing inlet velocities.

flow rate are compared in Fig. 12a and b, respectively. The dependency of h_r and η_r on the mass flow rate is similar with them on the flow velocity. Under same mass flow rate, larger increases of h_r under helical-fin-anchored mode and greater decreases of h_r under step-wall-stabilized mode were caused by the helical fins. The helical fin is capable of improving both the radiant heat flux and energy conversion efficiency through anchoring the flame in the inlet channel under relatively low inlet velocities. And maximum increments of 38% and 54% are achieved for h_r and η_r in this study.

Fig. 13 plotted the combustion efficiency defined as $\eta_c = \frac{(\dot{M}_{H_2} - \dot{m}_{H_{2,outlet}})}{\dot{M}_{H_2}}$, where $\dot{m}_{H_{2,outlet}}$ is the mass flow rate of residual hydrogen integrated over the outlet. η_c decreases with the increasing of the inlet velocity for both combustors, and a near 100% efficiency is achieved at the low velocities. A distinct falling stage is observed between $V_{in} = 86$ m/s and 94 m/s for the Step combustor, which corresponding to the leakage of hydrogen due to tip opening. With the aid of the helical fins, η_c of the Helix combustor improves compared with the Step combustor. The increment amplifies at larger V_{in}, and the largest increment of 9.7%, i.e., from 85.3% to 93.6%, is achieved at 102 m/s. Fig. 13 shows the averaged exhaust gas temperature T_{outlet} on the outlet, which is the determining factor for the efficiency of gas turbines [43]. With the increase of V_{in}, T_{outlet} initially increases and then drops, which is in accordance with the decreasing of heat loss (η_r) and heat release (η_c) shown in Fig. 12 and Fig. 13. With the combustion efficiency of the Helix combustor gaining more superiority over the Step combustor, T_{outlet} of the Helix combustor exceeds that of the Step combustor at $V_{in} = 40$ m/s. And the maximum increment of T_{outlet} is from 1314.3 K to 1415.7 K at $V_{in} = 102$ m/s. Variations of η_c and T_{outlet} with the increase of mass flow rate are also given in Fig. 13, which show the same tendencies depending on the inlet velocity. The improvement of η_c and T_{outlet} in the Helix combustor under the same mass flow rate is larger than that at the same inlet velocity.

Fig. 14a shows the profiles of hydrogen consumption ratio $R_c = \frac{\dot{M}_{H_2} - \dot{m}_{H_{2,Z}}}{\dot{M}_{H_2}}$ with the increase of V_{in}. Here $\dot{m}_{H_{2,Z}}$ is the mass flow rate of H_2 integrated over cross-sections perpendicular to the Z-axis. The Helix combustor has an overall higher R_c than the Step combustor, with the discrepancy increases firstly and then decreases when approaching the

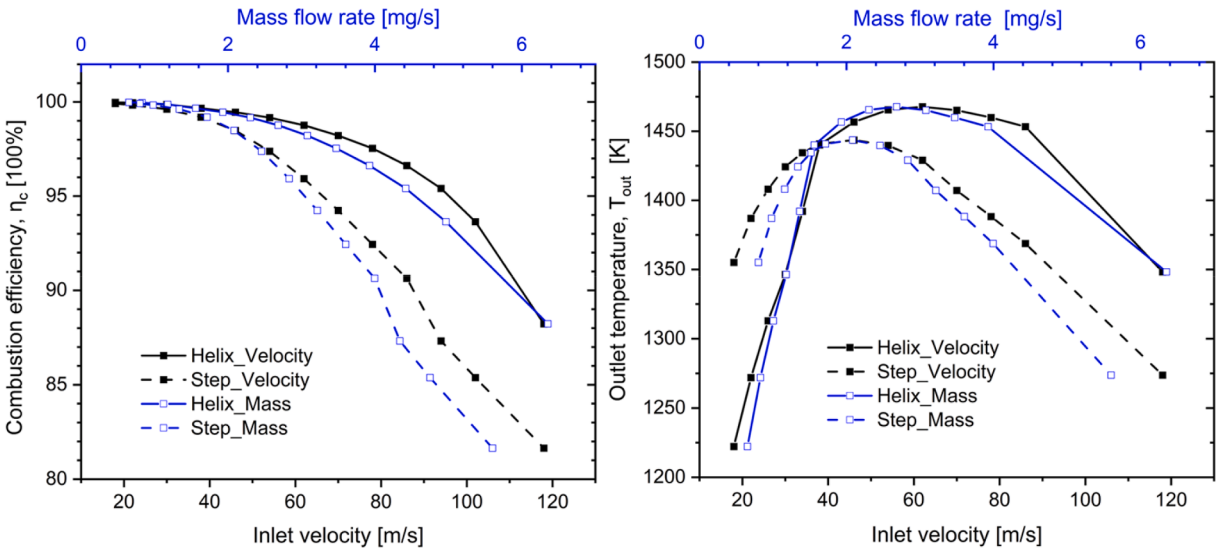

Fig. 13. The decline of combustion efficiency with increasing inlet velocity for the Helix and Step combustors.

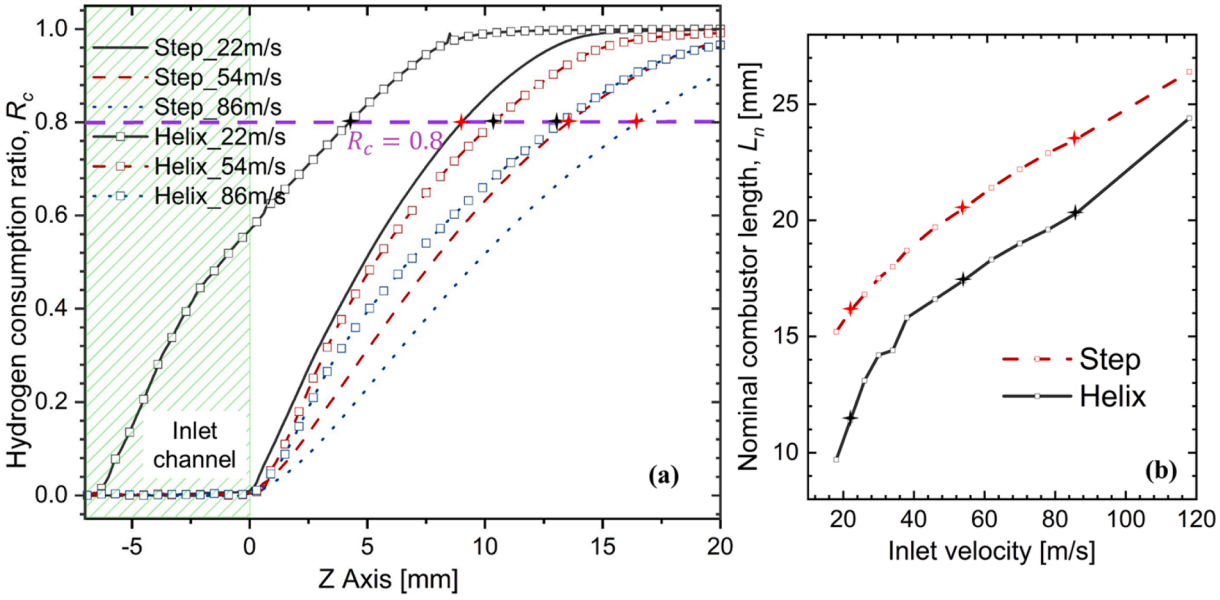

Fig. 14. (a) Hydrogen consumption ratio variations along the axis of the Helix and Step combustors at different inlet velocities. (b) The comparison of nominal combustor length versus inlet velocity of different combustors.

outlet. For the helical-fin-anchored flame, e.g., "Helix_22m/s", the discrepancy increases in the inlet channel where the flame anchored, while for the step-wall-stabilized flame the difference is enlarged near the step wall. With the receding of the enhance effect of helical fin, the reaction rate decreases when approaching the flame tip as shown in Fig. 4 and Fig. 7, leading to the decrease of the discrepancy ofR_c. The slopes of R_c curves decrease with the increasing of V_{in}, as the flow residence time for H_2 combustion is reduced. Noted that under relatively low velocities, R_c is consumed almost completely before the outlet, especially for the Helix combustor. The nominal combustor length L_n, which is defined as the distance from the inlet to the position where R_c = 0.8 is plotted in Fig. 14b to evaluate the potential of the helical fins in downscaling of the combustor. Compared with the Step combustor, L_n of the Helix combustor is prominently reduced, especially under the helical-fin-anchored flame mode. As the flame transforms to the step-stabilized mode with the increasing of V_{in}, a sudden rise of L_n is observed. The maximum decreasing ratios of L_n for two flame modes are 36.2% and 15.7%, respectively.

Based on above discussion, we can find that the Helix combustor shows great advantage as an emitter given the higher radiant energy and energy conversion efficiency at relatively low inlet velocities (under helical-fin-anchored mode). It also exhibits superiority in combustion efficiency and outlet temperature at higher inlet velocities (under step-wall-stabilized mode), suggesting its potential application in micro-engines.

4. Conclusions

This study proposed a novel helical-fin-assisted micro-step combustor. The performance of the proposed Helix combustor and the conventional micro-step combustor was compared. The effect of the helical fins on the flow and combustion characteristics was analyzed with the aid of detailed hydrogen-air chemistry and a conjugated heat transfer mode.

Two flame stabilization modes were observed in the Helix combustor with increasing inlet velocity. In the range of relatively low inlet velocities, the flame can be ignited by the high-temperature helical fins and stabilized in the inlet channel due to the preheating effect. At higher inlet velocities, the flame is transformed to the step-stabilized mode, where the swirl flow induced by the helical fins strengthens the mixing between the fresh mixture and high temperature products and considerably improves the combustion efficiency.

Under the helical-fin-flame model, the radiant power and the radiant energy conversion efficiency are significantly improved compared with the step combustor, with maximum ratios of 38% and 54%, respectively. Under higher inlet velocities, the flame is anchored behind the step wall. The combustion efficiency and the outlet temperature of the step-stabilized flame decrease with the increase of inlet velocity. The helical fins improve both the combustion efficiency and the outlet temperature. The maximum improvement is at 105 m/s, where the combustion efficiency increases from 85.3% to 93.6%, and the outlet temperature rises from 1314.3 K to 1415.7 K. Larger improvement was achieved under the same flow rate. Thus, the helical fin enhanced micro-step combustor has a high application potential as the emitter of MTPV systems under moderate flow rates. Furthermore, the helical fin broadens the applicability of micro-step combustor in micro-engines at higher inlet velocities. The application-oriented structural optimization of the Helix combustor for MPTV, micro-engine system or the integration of them will be carried out in future studies.

CRediT authorship contribution statement

Zheng Zhang: Methodology, Writing – original draft, Visualization, Investigation. **Wubingyi Shen:** Data curation, Visualization. **Wei Yao:** Writing – review & editing, Funding acquisition. **Qiu Wang:** Writing – review & editing. **Wei Zhao:** Supervision.

Declaration of Competing Interest

The authors declare that they have no known competing financial interests or personal relationships that could have appeared to influence the work reported in this paper.

Acknowledgments

The research was supported by National Key Research and Development Program of China (2019YFB1704200). The authors are also grateful to the National Supercomputer Center in Tianjin for providing the computational resource.

References

[1] Ju YG, Maruta K. Microscale combustion: technology development and fundamental research. Progr Energy Combust Sci 2011;37(6):669–715.
[2] Pizza G, Frouzakis CE, Mantzaras J, Tomboulides AG, Boulouchos K. Dynamics of premixed hydrogen/air flames in microchannels. Combust Flame 2008;152(3):433–50.
[3] Pokharel S, Ayoobi M, Akkerman Vy. Computational Analysis of Premixed Syngas/Air Combustion in Micro-channels: Impacts of Flow Rate and Fuel Composition. 2021;14(14):4190.
[4] Maruta K, Kataoka T, Kim NI, Minaev S, Fursenko R. Characteristics of combustion in a narrow channel with a temperature gradient. Proc Combust Inst 2005;30(2):2429–36.
[5] Wang S, Fan A. Combustion regimes of syngas flame in a micro flow reactor with controlled temperature profile: a numerical study. Combust Flame 2021;230.
[6] Dejoan A, Kurdyumov VN. Thermal expansion effect on the propagation of premixed flames in narrow channels of circular cross-section: multiplicity of solutions, axisymmetry and non-axisymmetry. Proc Combust Inst 2019;37(2):1927–35.
[7] Tang A, Cai T, Deng J, Zhao D, Huang Q, Zhou C. Experimental study on flame structure transitions of premixed propane/air in micro-scale planar combustors. Energy 2019;179:558–70.
[8] Kang X, Sun B, Wang J, Wang Y. A numerical investigation on the thermo-chemical structures of methane-oxygen diffusion flame-streets in a microchannel. Combust Flame 2019;206:266–81.
[9] Brambilla A, Schultze M, Frouzakis CE, Mantzaras J, Bombach R, Boulouchos K. An experimental and numerical investigation of premixed syngas combustion dynamics in mesoscale channels with controlled wall temperature profiles. Proc Combust Inst 2015;35(3):3429–37.
[10] Ayoobi M, Schoegl I. Numerical analysis of flame instabilities in narrow channels: Laminar premixed methane/air combustion. Int J Spray Combust Dyn 2017;9(3):155–71.
[11] Spalding DB. A theory of inflammability limits and flame-quenching. Proc R Soc London, Ser A 1957;240(1220):83–100.
[12] Ju Y, Xu Bo. Theoretical and experimental studies on mesoscale flame propagation and extinction. Proc Combust Inst 2005;30(2):2445–53.
[13] Leach TT, Cadou CP. The role of structural heat exchange and heat loss in the design of efficient silicon micro-combustors. Proc Combust Inst 2005;30(2):2437–44.
[14] Wan J, Fan A. Recent progress in flame stabilization technologies for combustion-based micro energy and power systems. Fuel 2021;286.
[15] Kang X, Veeraragavan A. Experimental investigation of flame stability limits of a mesoscale combustor with thermally orthotropic walls. Appl Therm Eng 2015;85:234–42.
[16] Alipoor A, Saidi MH. Numerical study of hydrogen-air combustion characteristics in a novel micro-thermophotovoltaic power generator. Appl Energy 2017;199:382–99.
[17] Zuo W, E J, Han D, Jin Yu. Numerical investigations on thermal performance of double-layer four-channel micro combustors for micro-thermophotovoltaic system. Energy Convers Manage 2017;150:343–55.
[18] Ni S, Zhao D, Becker S, Tang A. Thermodynamics and entropy generation studies of a T-shaped micro-combustor: effects of porous medium and ring-shaped ribs. Appl Therm Eng 2020;175:115374.
[19] Pan J, Zhu J, Liu Q, Zhu Y, Tang A, Lu Q. Effect of micro-pin-fin arrays on the heat transfer and combustion characteristics in the micro-combustor. Int J Hydrog Energy 2017;42(36):23207–17.
[20] Chen J, Yan L, Song W, Xu D. Effect of heat recirculation on the combustion stability of methane-air mixtures in catalytic micro-combustors. Appl Therm Eng 2017;115:702–14.
[21] Wang Y, Yang W, Zhou J, Yang H, Yao Y, Cen K. Heterogeneous reaction characteristics and their effects on homogeneous combustion of methane/air mixture in micro channels I. Thermal analysis. Fuel 2018;234:20–9.
[22] Brambilla A, Frouzakis CE, Mantzaras J, Tomboulides A, Kerkemeier S, Boulouchos K. Detailed transient numerical simulation of H2/air hetero-/homogeneous combustion in platinum-coated channels with conjugate heat transfer. Combust Flame 2014;161(10):2692–707.
[23] Sui R, Mantzaras J. Combustion stability and hetero-/homogeneous chemistry interactions for fuel-lean hydrogen/air mixtures in platinum-coated microchannels. Combust Flame 2016;173:370–86.
[24] Wan JL, Fan AW, Maruta K, Yao H, Liu W. Experimental and numerical investigation on combustion characteristics of premixed hydrogen/air flame in a micro-combustor with a bluff body. Int J Hydrog Energy 2012;37(24):19190–7.
[25] Bagheri G, Hosseini SE, Wahid MA. Effects of bluff body shape on the flame stability in premixed micro-combustion of hydrogen air mixture. Appl Therm Eng 2014;67(1–2):266–72.
[26] Niu JT, Ran JY, Li LY, Du XS, Wang RR, Ran MC. Effects of trapezoidal bluff bodies on blow out limit of methane/air combustion in a micro-channel. Appl Therm Eng 2016;95:454–61.
[27] Yan Y, He Z, Xu Q, Zhang Li, Li L, Yang Z, et al. Numerical study on premixed hydrogen/air combustion characteristics in micro–combustor with slits on both sides of the bluff body. Int J Hydrog Energy 2019;44(3):1998–2012.
[28] Pan J, Wang X, Lu Q, Chen L, Wang Y, Quaye EK. Effect of convex platform structure on hydrogen and oxygen combustion characteristics in micro combustor. Int J Hydrog Energy 2021;46(18):10973–83.
[29] Ben-Yakar A, Hanson RK. Cavity flame-holders for ignition and flame stabilization in scramjets: an overview. J Propul Power 2001;17(4):869–77.
[30] Li YH, Chen GB, Wu FH, Cheng TS, Chao YC. Effects of catalyst segmentation with cavities on combustion enhancement of blended fuels in a micro channel. Combust Flame 2012;159(4):1644–51.
[31] Wan J, Yang W, Fan A, Liu Yi, Yao H, Liu W, et al. A numerical investigation on combustion characteristics of H-2/air mixture in a microcombustor with wall cavities. Int J Hydrog Energy 2014;39(15):8138–46.
[32] Zhang Z, Wu K, Yuen R, Yao W, Wang J. Numerical investigation on the performance of bluff body augmented micro cavity-combustor. Int J Hydrog Energy 2020;45(7):4932–45.
[33] Gao W, Yan Y, Shen K, Huang L, Zhao T, Gao B. Combustion characteristic of premixed H2/air in the micro cavity combustor with guide vanes. Energy 2022;239:121975.
[34] Yang WM, Chou SK, Shu C, Li ZW, Xue H. Combustion in micro-cylindrical combustors with and without a backward facing step. Appl Therm Eng 2002;22(16):1777–87.
[35] Sahota GPS, Khandelwal B, Kumar S. Experimental investigations on a new active swirl based microcombustor for an integrated micro-reformer system. Energy Convers Manage 2011;52(10):3206–13.
[36] Khandelwal B, Deshpande AA, Kumar S. Experimental studies on flame stabilization in a three step rearward facing configuration based micro channel combustor. Appl Therm Eng 2013;58(1–2):363–8.
[37] Zarvandi J, Tabejamaat S, Baigmohammadi M. Numerical study of the effects of heat transfer methods on CH4/(CH4 + H-2)-AIR pre-mixed flames in a micro-stepped tube. Energy 2012;44(1):396–409.

[38] Peng Q, Wu Y, E J, Yang W, Xu H, Li Z. Combustion characteristics and thermal performance of premixed hydrogen-air in a two-rearward-step micro tube. Appl Energy 2019;242:424–38.
[39] Yilmaz I, Yilmaz H, Cam O, Ilbas M. Combustion characteristics of premixed hydrogen/air flames in a geometrically modified micro combustor. Fuel 2018;217:536–43.
[40] E J, Liu H, Zhao X, Han D, Peng Q, Zuo W, et al. Investigation on the combustion performance enhancement of the premixed methane/air in a two-step micro combustor. Appl Therm Eng 2018;141:114–25.
[41] Faramarzpour H, Mazaheri K, Alipoor A. Effect of backward facing step on radiation efficiency in a micro combustor. Int J Therm Sci 2018;132:129–36.
[42] Spadaccini CM, Mehra A, Lee J, Zhang X, Lukachko S, Waitz IA. High power density silicon combustion systems for micro gas turbine engines. J Eng Gas Turbines Power-Trans Asme 2003;125(3):709–19.
[43] Cao HL, Xu JL. Thermal performance of a micro-combustor for micro-gas turbine system. Energy Convers Manage 2007;48(5):1569–78.
[44] Li J, Chou SK, Huang G, Yang WM, Li ZW. Study on premixed combustion in cylindrical micro combustors: transient flame behavior and wall heat flux. Exp Therm Fluid Sci 2009;33(4):764–73.
[45] Ni S, Zhao D, Zhu X. Heat transfer and entropy production evaluation on premixed hydrogen/air-fuelled micro-combustors with internal threads. Fuel 2021;303:121325.
[46] He Z, Yan Y, Zhao T, Feng S, Li X, Zhang L, et al. Heat transfer enhancement and exergy efficiency improvement of a micro combustor with internal spiral fins for thermophotovoltaic systems. Appl Therm Eng 2021;189:116723.
[47] Yang X, Yang W, Dong S, Tan H. Flame stability analysis of premixed hydrogen/air mixtures in a swirl micro-combustor. Energy 2020;209:118495.
[48] Li ZW, Chou SK, Shu C, Yang WM. Effects of step height on wall temperature of a microcombustor. J Micromech Microeng 2005;15(1):207–12.
[49] Norton DG, Vlachos DG. A CFD study of propane/air microflame stability. Combust Flame 2004;138(1–2):97–107.
[50] De Santis A, Ingham DB, Ma L, Pourkashanian M. CFD analysis of exhaust gas recirculation in a micro gas turbine combustor for CO2 capture. Fuel 2016;173:146–54.
[51] Yang X, Zhao L, He Z, Dong S, Tan H. Comparative study of combustion and thermal performance in a swirling micro combustor under premixed and non-premixed modes. Appl Therm Eng 2019;160:114110.
[52] Li J, Zhao Z, Kazakov A, Dryer FL. An updated comprehensive kinetic model of hydrogen combustion. Int J Chem Kinet 2004;36(10):566–75.
[53] Kee RJ, Rupley FM, Miller JA. The chemkin thermodynamic data base. Sandia Report SAND 1990;87.
[54] Kee RJ, Dixon-Lewis G, Warnatz J, Coltrin ME, Miller JAJSNLRS-. A Fortran computer code package for the evaluation of gas-phase multicomponent transport properties. Sandia National Laboratories Report SAND86-8246 1986;13:80401-1887.
[55] Bergman TL, Incropera FP, DeWitt DP, Lavine AS. Fundamentals of heat and mass transfer. John Wiley & Sons; 2011.
[56] Holman J. Heat transfer. 10th ed. New York: Mc-GrawHill Higher Education; 2010.
[57] Kuo CH, Ronney PD. Numerical modeling of non-adiabatic heat-recirculating combustors. Proc Combust Inst 2007;31(2):3277–84.
[58] Fureby C. Subgrid models, reaction mechanisms, and combustion models in large-eddy simulation of supersonic combustion. AIAA J 2020;59(1):215–27.
[59] Bazooyar B, Gohari Darabkhani H. Analysis of flame stabilization to a thermo-photovoltaic micro-combustor step in turbulent premixed hydrogen flame. Fuel 2019;257:115989.
[60] Peng Q, Jiaqiang E, Yang WM, Xu H, Chen J, Zhang F, et al. Experimental and numerical investigation of a micro-thermophotovoltaic system with different backward-facing steps and wall thicknesses. Energy 2019;173:540–7.
[61] Sanchez AL, Williams FA. Recent advances in understanding of flammability characteristics of hydrogen. Progr Energy Combust Sci 2014;41:1–55.
[62] Melguizo-Gavilanes J, Boeck LR, Mével R, Shepherd JE. Hot surface ignition of stoichiometric hydrogen-air mixtures. Int J Hydrog Energy 2017;42(11):7393–403.
[63] Boeck LR, Melguizo-Gavilanes J, Shepherd JE. Hot surface ignition dynamics in premixed hydrogen–air near the lean flammability limit. Combust Flame 2019;210:467–78.
[64] Gabruk RS, Roe LA. Velocity characteristics of reacting and nonreacting flows in a dump combustor. J Propul Power 1994;10(2):148–54.
[65] Hong S, Shanbhogue SJ, Ghoniem AF. Impact of fuel composition on the recirculation zone structure and its role in lean premixed flame anchoring. Proc Combust Inst 2015;35(2):1493–500.